Journal of Materials Chemistry A

PAPER

View Article Online
View Journal | View Issue

Cite this: J. Mater. Chem. A, 2015, 3, 11478

Ordered mesoporous titania from highly amphiphilic block copolymers: tuned solution conditions enable highly ordered morphologies and ultra-large mesopores†

Morgan Stefik,‡*[a] Juho Song,‡[bc] Hiroaki Sai,§[b] Stefan Guldin,[d] Patrick Boldrighini,[b] M. Christopher Orilall,[b] Ullrich Steiner,[e] Sol M. Gruner[f] and Ulrich Wiesner*[b]

Received 6th April 2015
Accepted 21st April 2015

DOI: 10.1039/c5ta02483h

www.rsc.org/MaterialsA

Crystalline transition metal oxides with controlled mesopore architectures are in increasing demand to enhance the performance of energy conversion and storage devices. Solution based block copolymer self-assembly routes to achieve ordered mesoporous and crystalline titania have been studied for more than a decade, but have so far mostly been limited to water and alcohol dispersible polymers. This constraint has limited the accessible morphology space as well as structural dimensions. Moreover, synthetic approaches are mostly performed in a trial-and-error fashion using chemical intuition rather than being based on well-defined design parameters. We present solubility design guidelines that facilitate coassembly with highly amphiphilic block copolymers, enabling the formation of ordered structures with diverse length scales (d_{10} = 13.8–63.0 nm) and bulk-type morphologies. Thus, highly ordered and crystalline titania with the largest reported pores (d = 32.3 nm) was demonstrated for such a coassembly approach without the use of pore-expanders. Furthermore, the use of an ABC triblock terpolymer system led to a 3D ordered network morphology. In all cases, subsequent calcination treatments, such as the CASH procedure, enabled the formation of highly crystalline mesoporous materials while preserving the mesostructure.

Introduction

Significant efforts have focused on the control of transition metal oxide nanostructures which have a diverse range of (photo)catalytic, transport (electron/ion), electronic (insulator/semiconductor/conductor), and optical properties. Indeed, transition metal oxide nanostructures are of great interest for numerous applications including, *e.g.*, batteries, supercapacitors, dye-sensitized solar cells, photoelectrochemical water splitting devices, fuel cells, and electrochromic devices.[1–9] For all of the above catalysis and electrochemistry uses, the material performance is largely dictated by the nature and availability of surfaces. Thus the role of morphology on the nanoscale plays a significant role on device performance. Among the many transition metal oxides, titania is one of the most popular due to its use in the whole range of applications mentioned above.[10,11]

Over the past two decades significant advances have been made in the fabrication of ordered inorganic materials with organic structure-directing agents (SDA). Typically amphiphilic SDAs are used where a selective interaction such as electrostatics or hydrogen bonding selectively associate the hydrophilic inorganic entities with the hydrophilic portion of the SDA. At the same time, the hydrophobic portion of the SDA phase separates from the hydrophilic components with nanoscale periodicity. Under certain controlled conditions the free energy balance of the inorganic-SDA coassembly leads to the equilibration of highly ordered nanoscale domains. The first example of such an approach utilized a surfactant to swell the spacing between ordered kanemite sheets in 1990.[12] This concept was then greatly expanded to enable the assembly of

[a]Department Chemistry and Biochemistry, University of South Carolina, Columbia, SC 29208, USA. E-mail: morgan@stefikgroup.com
[b]Department of Materials Science and Engineering, Cornell University, Ithaca, New York 14853, USA. E-mail: ubw1@cornell.edu
[c]School of Chemical and Biomolecular Engineering, Cornell University, Ithaca, New York 14853, USA
[d]Department of Chemical Engineering, University College London, Torrington Place, London, WC1E 7JE, UK
[e]Adolphe Merkle Institute, University of Fribourg, Chemin des Verdiers, Fribourg, CH-1700, Switzerland
[f]Department of Physics, Cornell University and Cornell High Energy Synchrotron Source, Ithaca, New York 14853, USA

† Electronic supplementary information (ESI) available: *In situ* SAXS data, additional SEM, TEM, XRD, SAXS, and physisorption data, as well as a table summary of calcination conditions. See DOI: 10.1039/c5ta02483h

‡ These authors contributed equally to this work.

§ Present address: Center for Bio-inspired Energy Science, Northwestern University, Evanston IL, 60208

other silicate materials with multiple ordered morphologies by utilizing micellar surfactant assemblies.[13]

The controlled coassembly of transition metal oxides with SDAs is more difficult than silicates due to the multiple stable coordination states and much greater chemical reactivity (*e.g.* hydrolysis of $Ti(OR)_4$ is 10^5 times faster than $Si(OR)_4$).[14] Hydrolytic sol–gel routes were typically employed under acidic conditions that promote hydrolysis and severely slow the condensation reactions to allow time for coassembly with the SDA before gelation. Chelating ligands and non-hydrolytic sol–gel approaches have also been employed to slow these reaction rates. Although metal oxides other than titania were first accomplished,[15] similar methodologies later yielded ordered titania nanostructures.[16] Often the SDAs were removed from such hybrid materials to yield micro/mesoporous materials (IUPAC pore-size naming convention[17,18]) preserving the ordered inorganic morphology. The pore sizes in surfactant-based materials were typically ~1–5 nm due to the small molar mass of the SDA (~150–350 g mol^{-1}). This limited range of pore sizes was expanded up to ~7 nm for ordered pores and up to 12 nm for irregular pores by swelling the hydrophobic domains with hydrophobic "pore-expanding" molecules.[19]

Amphiphilic block copolymers are able to circumvent this feature size limitation with larger SDA molar masses (~1000–70 000 g mol^{-1}). Most block copolymer SDAs utilize a non-ionic poly(ethylene oxide) block to coordinate with the inorganic species.[20,21] Block copolymers were first applied in the structure-directed manufacture of ordered silicates[22,23] and were then employed as SDAs with many transition metal oxides, including titania.[24] Pluronic poly(ethylene oxide-*b*-propylene oxide-*b*-ethylene oxide), (PEO-*b*-PPO-*b*-PEO)s are commercially available and thus commonly used polymers of relatively low molar mass, ~2000–13 000 g mol^{-1} [25] (Table 1). It follows that the resulting ordered oxide structures typically had 4–7 nm pores which were only slightly larger than those obtained from conventional surfactants. Similar to surfactants, larger pores were observed in disordered films[26] or when pore expanders were added.[27]

Many applications utilizing transition metal oxides require the electronic or catalytic properties of specific crystal structures. Thus, significant effort was directed towards crystallization heat treatments of the amorphous transition metal oxide structures that typically result from hydrolytic sol–gel processes. Such heat treatments of titania films structure-directed with Pluronics are typically limited to low temperatures which result in anatase crystallites embedded in amorphous walls.[24] Although Pluronic SDAs can lead to highly crystalline ordered titania nanostructures when supported thin films were calcined, there remains a general challenge to achieve highly crystalline and ordered bulk materials.[28–30] Successful crystallization requires the good interconnection of amorphous oxide particles and resulting crystallite sizes that are comparable to the wall thickness.

An alternative polymeric SDA is based on hydrogenated poly(butadiene-*b*-ethylene oxide) and is termed KLE. It yields mesoporous materials with thicker walls that enabled higher temperature processing which resulted in larger crystallites and reduced amorphous content. For example, KLE led to mesoporous titania thin films with 10 nm pores that were stable up to 600 °C.[31,32] KLE polymers have similar molar masses as Pluronics, but have a much larger Flory–Huggins monomer–monomer interaction parameter, χ. The resulting increased enthalpic penalty for A–B interfacial contacts between the KLE blocks offsets the entropic penalty for chain stretching, leading to slightly larger mesostructures than Pluronic polymers. However, only spherical micellar morphologies have been demonstrated with KLE SDAs thus far.[31–33] There are indeed numerous reports of coassembled titania with block copolymers.[3,16,24,26–58]

The achievement of larger nanostructures and/or novel ordered morphologies requires the development of new SDAs.[59] The combination of creative polymer chemistry with inorganic/solid-state chemistry is likely to ultimately yield the biggest benefits for SDA-based approaches. Most polymers are hydrophobic, however, and are thus immiscible with the typically used alcohol and water based sol–gel processes (in fact water and alcohol are commonly used as precipitation agents for polymers). The coassembly of titania with poly(styrene-*b*-ethylene oxide) (PS-*b*-PEO) in the presence of these poor solvents lead to either disordered structures[55,60,61] or to ordered macroporous emulsions.[62] Although PS-*b*-PEO has also coassembled ordered nanostructures under certain conditions, there is not yet a systematic framework for developing new coassembly systems with highly amphiphilic block copolymers.[63–65] The formation of equilibrated bulk morphologies

Table 1 Comparison of three structure-directing agents for ordered mesoporous silicates[a]

	Pluronic PEO-*b*-PPO-*b*-PEO	KLE PHB-*b*-PEO	IO PI-*b*-PEO
Flory–Huggins χ at 50 °C	0.085 [104]	~0.33*	0.33 [105]
Mn (kg mol^{-1})	2–13 [25]	8–10 [106]	10–84 [107]
wt% PEO	30–70% [25]	37–57% [106]	8–38% [107]
Water/alcohol soluble	Yes	Yes**	No
Hybrid morphologies	CM, iH, G, L[39,108]	CM[106]	CM, iCM, H, iH, PN, G, L[67]
Pore size range*** (nm)	5–10 [23]	12–13 [106]	11–50 [107]

[a] CM = cubic packing of spherical micelles, L = lamellar, H = hexagonally arranged cylinders, G = double gyroid, PN = plumber's nightmare. *χ for KLE is similar to that for IO. **PHB and PI homopolymers are not soluble in water or alcohols, but can be dispersed as aggregates in such solvents when of low molar mass and attached to a large fraction of PEO. ***Ordered mesopores without pore-expanders.

based on block copolymer thermodynamics requires that the polymer does not become trapped in a selective solvent-induced morphology such as spherical micelles. Another example are the ~30 000 g mol^{-1} and highly amphiphilic poly(isoprene-*b*-ethylene oxide)s (PI-*b*-PEO) with majority PI blocks which were recently used to structure-direct inverse-hexagonal niobium oxide and worm-like titania nanostructures.[66] The use of non-hydrolytic sol–gel processes and organic solvents were key to enabling solvent evaporation-induced coassembly with these hydrophobic polymers. In the same study, the so called combined assembly by soft and hard chemistries (CASH) approach enabled oxide crystallization without structure collapse by the *in situ* creation of a hard template from the carbon which resulted from polymer pyrolysis under an inert atmosphere. The carbon was subsequently removed, yielding crystalline oxide nanostructures with large ~24 nm pores and 10 nm thick walls. While 8 different morphologies were demonstrated with PI-*b*-PEO SDAs in aluminosilicates,[67] including bicontinuous networked structures,[68–71] this morphological diversity is currently lacking in titania nanostructures. Finally, an emerging trend to achieve ordered network morphologies is based on ABC triblock terpolymer SDAs which have large composition windows for network coassembly.[72] Here again, better control of the evaporation-induced structure formation is needed to fully realize the morphological diversity of triblock terpolymer self-assembly with transition metal oxides, including access to large pore mesoporous materials.

From all of the above examples, it is apparent that there is a need to develop a better understanding of the thermodynamic processes that control (transition metal) oxide structure formation directed from large molar mass SDAs in different solvents. In particular, it is desirable to establish quantitative, or at least semi-quantitative guidelines for successful structure formation, replacing chemical intuition-based trial and error. Toward this end, we provide a framework to semi-quantitatively describe the solvent evaporation-induced coassembly of titania into ordered bulk-type morphologies using highly amphiphilic block copolymers over a broad range of molar masses. This framework, which is based on solubility parameters, provides experimental guidelines to avoid kinetically trapped solution structures (such as spherical micelles) thereby enabling the fine-tuning of titania nanostructures and pore sizes. This semi-quantitative approach allowed us to achieve a highly ordered crystalline titania structure with the largest reported cylindrical mesopores to date without the use of pore-expanding agents. The extension of this approach from simple AB diblock copolymers to ABC triblock terpolymers with ordered network nanostructures suggests that this framework may be generalizable to other new SDAs.

Experimental procedures

Reagents. Tetrahydrofuran (THF, HPLC grade, J.T. Baker) was stored over activated 3 Å molecular sieves until use, or anhydrous tetrahydrofuran (>99.9%, Aldrich) was used as received. Titanium isopropoxide (97%, Aldrich) and concentrated hydrochloric acid (37 wt% ACS grade, BDH Aristar) were used as received. Block copolymers were prepared by anionic polymerization using reported procedures.[73,74] Poly(-isoprene-*b*-ethylene oxide)s (PI-*b*-PEO) were synthesized with different molar masses from 7 to 92 kg mol^{-1}. They are termed as IO*x*K, with *x* denoting the polymer molar mass in kg mol^{-1}. Characterization results are summarized in Table 2. All polymers showed narrow molar mass distributions with PDIs (polydispersity index) less than 1.11. Poly(isoprene-*b*-styrene-*b*-ethylene oxide) (ISO1) was synthesized as described elsewhere[75] with a molar mass of 53.4 kg mol^{-1} containing 14.6 kg mol^{-1} of PI, 29.0 kg mol^{-1} of PS, and 9.8 kg mol^{-1} of PEO and a PDI of 1.05.

Hybrid synthesis. Block copolymers were dissolved in THF with stirring for at least 1 hour. Hydrochloric acid was then added to the polymer solution followed by titanium isopropoxide. The resulting orange to red solution was stirred for 24 h during which the solution turned slightly yellow to clear. The solution was cast into an 8 cm Teflon dish which was placed onto a glass dish on a hotplate to slow the loss of HCl due to reaction with the steel hotplate surface. This assembly was then covered with a glass hemisphere to slow evaporation and limit exposure to ambient humidity. The hot plate was set to 50 °C creating an effective casting temperature of ~40 °C. After 24 h of drying, the films were placed into an oven set to 100 °C for a minimum of 3 days to enhance the condensation reaction. The films were then subjected to calcination heat treatments to crystallize the titania. Crystallization was induced either in air to oxidatively remove the polymer or in nitrogen to convert the polymer into a carbonaceous framework using the CASH approach, *vide supra*. The inverse hexagonal hybrids were heated to 700 °C and the networked hybrids were heated to 400 °C. The carbon residue in some composites was subsequently removed by heating to 450 °C in air for at least 1 hour. All heat treatments utilized a 1–5 °C min^{-1} heating ramp rate with a 1–4 hour hold followed by letting the furnace cool to room temperature.

As-made samples prepared with IO28K are termed IO28K-h*x* where *x* is the wt% of water in the THF solution prior to addition of the titanium isopropoxide. These casting solutions were all prepared with 50 mg of IO28K, 0.119 mL HCl(aq), 0.371 mL titanium(IV) isopropoxide, and the quantity of THF required to yield *x* wt% water in the solution. Thus 2.44, 3.28, 4.97, and 9.27

Table 2 Synthesis and characterization of PI-*b*-PEO block copolymers

	IO7K	IO13K	IO28K	IO41K	IO92K
Overall M_n, g mol^{-1}	6787	12 500	27 975	40 981	91 900
PI, g mol^{-1}	4410	9948	20 230	30 121	63 227
PEO, g mol^{-1}	2377	2552	7745	10 860	28 673
PDI	1.11	1.10	1.06	1.07	1.09
χN[a]	39.2	67.3	156.0	227.3	521
R_o of PEO[b], nm	4.4	4.5	7.9	9.3	15.2

[a] χN was calculated using $\chi = 65/T + 0.125$. [b] R_o was calculated based on the equation, $R_0 = 0.595\sqrt{N}$.

mL of THF were used to prepare the samples IO28K-h4, IO28K-h3, IO28K-h2, and IO28K-h1 with 4.0, 3.0, 2.0 and 1.08 wt% water, respectively. Note that the molar ratios for all recipes had Ti : H_2O : HCl of 1.0 : 4.0 : 1.16 which corresponds to the minimum water content required for the complete hydrolysis of the titanium alkoxide.

Pore size control experiments used different molar mass PI-*b*-PEOs and employed an *ex situ* sol–gel route. 50 mg of PI-*b*-PEO was dissolved in 8 mL of THF with stirring for about 1 hour. A titanium-containing sol was prepared separately by the addition of 0.4 mL titanium(IV) isopropoxide to 0.129 mL hydrochloric acid (37%) under vigorous stirring followed by addition of 2 mL THF after 5 min stirring. After another 5 min, the sol was added to the polymer solution followed by stirring for one hour. Then the films were cast and annealed as described before.

Hybrids from ISO1 were prepared similarly. 75 mg of ISO1 was dissolved in 2.9 mL of dry THF with stirring for at least 1 h. A dilute sol stock solution was prepared to enable accurate addition of a small quantity of titania: 5 mL of titanium isopropoxide was added to a quickly stirred vial containing 1.6 mL of concentrated HCl(aq). The vial was closed after combining alkoxide with acid and was left to stir for 5 min before 10 mL of dry THF was added to dilute the sol (orange color) and left to stir for an additional 2 min. A syringe was used to immediately measure 0.388 mL of the dilute sol stock solution and the aliquot was added directly to the stirred polymer solution. This combined solution was left to stir for at least 30 min and was then cast as previously described for the IO28K-h*x* samples. After 24 h, the film was placed into an oven set to 100 °C for 3 days to enhance the condensation reaction. Portions of this film were calcined under different temperature and atmospheric conditions to optimize the crystallization process while preserving the ordered mesostructure. Samples ISO1–N_2 and ISO1–air were both prepared directly from sample ISO1–TiO_2 by heating at 1 °C min^{-1} to 400 °C with a 1 h hold followed by letting the furnace cool in N_2 or air, respectively.

Characterization

TEM. Ultrathin ~70 nm sections were prepared with wet cryo microtoming using a Leica UC7/FC7 cryo-ultramicrotome. Sections were cut at −55 °C onto a 60 : 40 dimethylsulfoxide : water solution and then transferred to bare copper grids. A FEI Tecnai T12 twin transmission electron microscope was operated at 120 kV for microscopic inspection of the ultrathin sections. A Gatan Orius dual-scan CCD was used for image acquisition.

SEM. A Zeiss LEO 1550 SEM with a field emission source was utilized to acquire images of calcined samples using an acceleration voltage of 2 kV and an in-lens secondary electron detector.

SAXS. Small-angle X-ray scattering (SAXS) patterns of samples were obtained at the Cornell High Energy Synchrotron Source (CHESS) G1 station with a beam energy of 9 keV as well as at a home-built Rigaku RU300 Cu Kα rotating anode beamline. The details of both SAXS beamline configurations are described elsewhere.[72] For acquiring time-resolved SAXS patterns at the CHESS G1 station, portions of films were transferred from Teflon dishes to 1.0 mm glass capillaries or on a Kapton tape immediately before the measurements. The degree of solvent evaporation at each time point was estimated by measuring the weight of the film in the dish. Acquired 2D patterns were radially integrated around the beam center to produce plots of intensity *versus* scattering vector magnitude, q, defined as $q = 4\pi \sin\theta/\lambda$, where 2θ is the total scattering angle and λ is the X-ray wavelength.

Physisorption. Nitrogen physisorption isotherms were measured at −196 °C using a Micromeritics ASAP 2020 system. All samples were degassed under high vacuum at 150 °C overnight. The Brunauer, Emmett, and Teller (BET) and Brunauer, Jonyer, and Halenda (BJH) analyses were performed using the Micromeritics ASAP 2020 V1.05 software.[76,77]

XRD. Wide-angle X-ray diffraction measurements were performed using a Rigaku Ultima VI diffractometer at 40 kV and 44 mA where samples were scanned from 10 to 90 degrees with a 5 degrees min^{-1} speed.

Results and discussion

Solvent evaporation-induced structure formation

The dissolution of an SDA and an inorganic material is the fundamental first step towards their evaporative coassembly. However, typical hydrolytic sol–gel protocols for the coassembly of ordered titania films start with ~2–21 wt% SDA solutions of Pluronic[39,54] or KLE[33] in ethanol with ~8–21 wt% water. Such alcohol and water rich solutions are incompatible with the dissolution of a tremendous diversity of other potential polymer systems, including most derivatives of acrylates, methacrylates, styrenes, or dienes. The solubility of a particular component may be predicted from the Hildebrand solubility parameter (δ) which for a given molecule is the square root of its cohesive energy density and is measured in SI units of $\sqrt{(J\ m^{-3})}$ or equivalently in $\sqrt{Pa}$. Most δ values range from 14.9 to 47.9 $\sqrt{MPa}$, intermediate between hexanes and water, respectively (Fig. 2).[78] Ethanol with δ = 26.6 $\sqrt{MPa}$ is too hydrophilic to dissolve many common polymers such as polyisoprene, polystyrene, or poly(methyl methacrylate) (δ = 16.5, 18.6, and 22.7 $\sqrt{MPa}$, respectively). However, the simple substitution of ethanol with common hydrophobic solvents such as hexane, toluene, or chloroform (δ = 14.9, 18.2, and 19.0 $\sqrt{MPa}$ respectively) leads to the precipitation of the titania sol since these solvents do not hydrogen bond. The solubility parameter for acetylacetonate modified titania particles[79] and bare rutile particles[80] are 20.5 and 30.1$\sqrt{MPa}$, respectively. The dissolution of all species requires the selection of a solvent or a mixture of solvents with a similar δ value and an appropriate hydrogen bonding strength. Therefore solvents such as THF with a low δ = 18.6 $\sqrt{MPa}$ value and a moderate ability to hydrogen bond should be appropriate for many systems involving hydrophobic polymer blocks (Fig. 2). Indeed, THF is a good solvent for many polymers including all of those mentioned above and for this reason is one of the most common eluent solvents for gel permeation chromatography of polymers. As a result, THF was

chosen as the principal solvent for the coassembly of titania sols with the highly amphiphilic PI-*b*-PEO.

Dissolution of all coassembled species is required but not sufficient for the formation of equilibrated coassemblies. For example, the water associated with hydrolytic sol–gel processes may concentrate in the solution as volatile organic solvents often evaporate preferentially, leading to the precipitation of hydrophobic polymers. The measured precipitation point for IO28K is ~4.1 wt% water in THF determined using HCl(aq). Additionally, the composition of a mixed solvent system must remain favorable for all species present throughout the entire evaporation process. Relative evaporation rates and any azeotropic conditions should be considered for such mixed solvent systems.[81] For example, mixtures of THF and water at atmospheric pressure form an azeotrope with a lowered boiling point of 64 °C and a composition of 5.3 wt% water. Note however that deviations from the azeotropic temperature or the addition of other reagents may change the relative evaporation rates. The recipe for sample IO28K-h4 was adapted from reported titania coassembly protocols with the simple substitution of THF in place of ethanol. Note that before the addition of titanium isopropoxide the solution was close to, but slightly below, the threshold for polymer precipitation (4% *vs.* 4.1%, respectively). Hydrolysis is expected to proceed quickly once the alkoxide is added, consuming all of the free water ($TiR_4 : H_2O = 4.0 : 1.0$),[14] although some of this consumed water is expected to be released during the slow condensation reaction while stirring and casting. The initially orange color fading to clear overtime is consistent with initial THF coordination to the *in situ* formed $Ti(O^iPr)_aCl_b(OH)_{4-a-b}$ followed by reduction in coordination as the sol particles grow, lowering specific surface area.[82]

A titania : PI-*b*-PEO mass ratio of 2.0 : 1.0 was chosen to result in an inverse hexagonal (iH) morphology based on the previously established morphology map for the coassembly of PI-*b*-PEO with an aluminosilicate sol.[67] However, bright field TEM images of the resulting film show hollow dark circles consistent with an inverse spherical micelle (iSM) morphology containing PI cores (light) and PEO–TiO_2 coronas (dark) (Fig. 1b and c). Quantitative TEM image analysis indicated that these crew cut micelles had a diameter of 30 ± 3 nm, similar to the value obtained from the primary peak located at $q^* = 0.23$ nm^{-1} in SAXS measurements (Fig. 1a), corresponding to a spacing of 27 nm. A broad second peak was also observed at approximately twice the reciprocal spacing of the first peak. These are too few peaks to make an unambiguous morphology assignment on the basis of SAXS alone. Hence, in this and other similar cases the morphology assignments were made on the basis of the greatest consistency between the SAXS and electron microscopy data. For example, the SAXS in Fig. 1a was consistent with a simple cubic lattice, but not with either BCC nor FCC packing. However, long-range order was not apparent in the TEM observations, so the second SAXS peak was attributed to

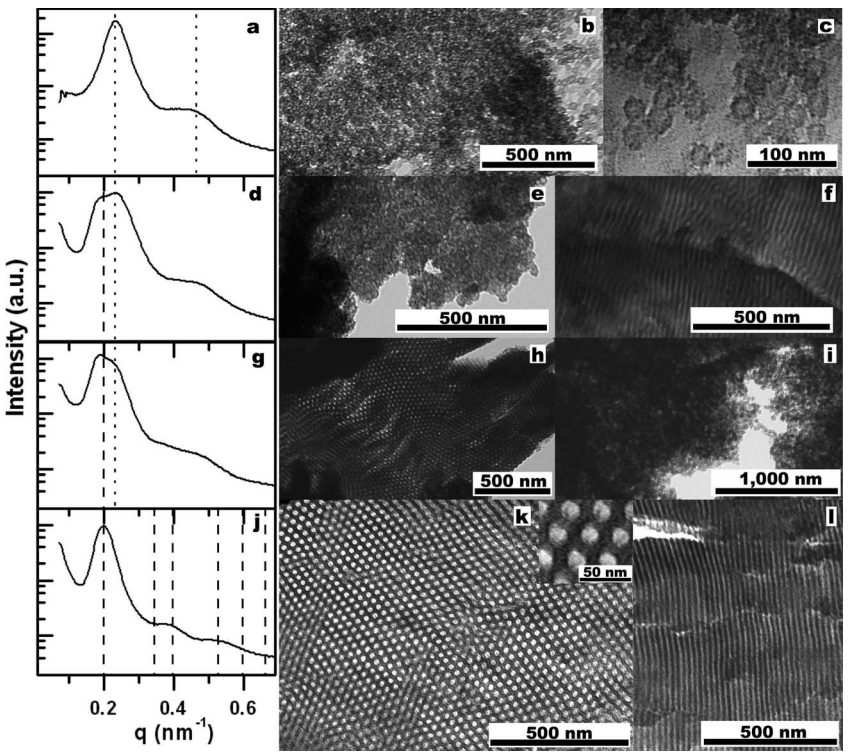

Fig. 1 The SAXS patterns for samples IO28K-h4 (a), IO28K-h3 (d), IO28K-h2 (g), and IO28K-h1 (j) indexed with a random micellar lattice (dots), a hexagonal lattice (dashes), or a mixture of the two. Bright field TEM images of IO28K-h4 (b and c), IO28K-h3 (e and f), IO28K-h2 (h and i), and IO28K-h1 (k and l) are consistent with inverse spherical micelles (iSM), inverse hexagonally arranged cylinders (iH), or a mixture of the two. The iH samples were indexed as $q/q^* = 1, \sqrt{3}, \sqrt{4}, \sqrt{7}, \sqrt{9}, \sqrt{12}$ where q is defined as $q = 4\pi \sin\theta/\lambda$. The data are presented as rows for each sample descending in order of increasing THF content (decreasing water fraction).

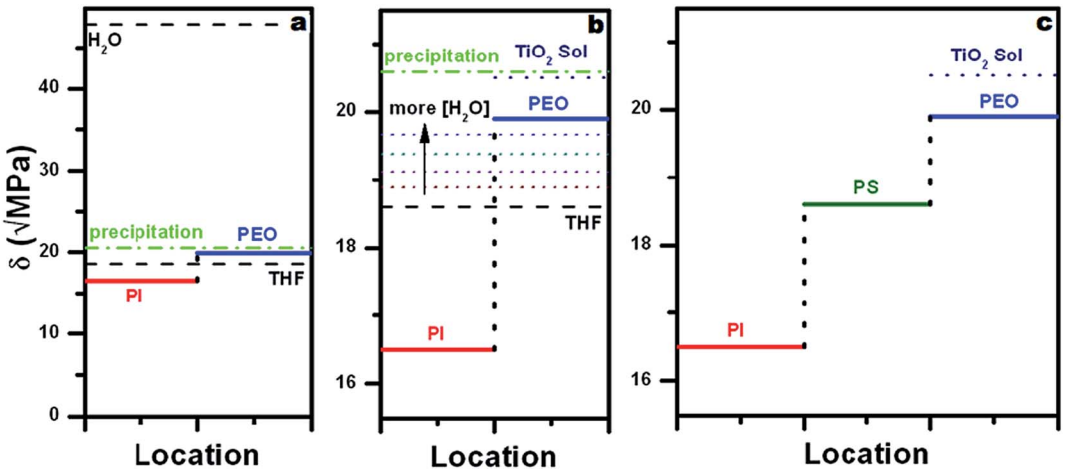

Fig. 2 Plots of Hildebrand solubility parameters indicating the relative strength of intermolecular interactions and facilitating the prediction of miscibility. Though water is a precipitation agent for many polymers, its use is required for numerous hydrolytic sol–gel procedures (a). Samples IO28K-h1, IO28K-h2, IO28K-h3, and IO28K-h4 were prepared with increasing initial water concentrations (b) leading to strikingly different morphologies (compare to Fig. 1). Successful coassembly with more complex triblock terpolymer structure directing agents requires attention to the solubility of all four species involved (c).

random packing of spheres. Extensive previous experiments indicate that the utilized IO28K should result in about 16 nm diameter iH cylinders. The larger than expected micelle diameters and deviation from the expected morphology suggest that sample IO28K-h4 was not equilibrated at the time of inorganic cross-linking, but was trapped in the solution morphology due to solvent selectivity of the PEO phase.

Solvent composition plays a key role as the polymer system transitions from solution dynamics to condensed matter behavior ("bulk").[83,84] If the solvent composition is favorable for all components, *i.e.*, non-selective, then the block copolymer chains exist as non-aggregated unimers evenly distributed throughout the solution. Consequently, the hybrid would gradually enter bulk behavior from a random mixed state. In contrast, when the solvent composition favors one portion of an amphiphilic polymer, the solvophobic blocks aggregate leading to micelle formation, typically with a spherical morphology. Published examples indicate that the addition of 3–11 wt% of a selective solvent to a block copolymer solution in a non-selective solvent is sufficient to induce micellization, depending on the particular blocks, block lengths, and solvents involved.[83,85–87] Indeed, the IO28K used in this study was significantly longer (28 kg mol^{-1}) and more hydrophobic (72 wt% PI), than the block copolymers typically used for micellization studies. One may anticipate this polymer should be more sensitive to the presence of selective hydrophilic solvents, *vide infra*.

To elucidate the role of residual water during film casting, several nearly identical films were prepared, only varying the quantity of THF added. With increasing THF content, the starting weight fraction of water was lowered sequentially from IO28K-h4, IO28K-h3, IO28K-h2, to IO28K-h1. The iSM morphology of the sample with the least THF, IO28K-h4, was already described, *vide supra*. Before describing the intermediate samples, we focus on IO28K-h1, the sample with the most THF added, *i.e.* the lowest water concentration. The SAXS pattern for IO28K-h1 was consistent with an inverse hexagonally arranged cylinders (iH) morphology (Fig. 1j), with the primary peak at $q^* = 0.20$ nm^{-1}. The allowed peaks for hexagonal symmetry are indicated in the figure at $(q/q^*)^2 = 1, 3, 4, 7, 9$ and 11. Additionally, significant sample texturing was evidenced by a pair of spots for $(q/q^*)^2 = 4$ peaks (data not shown). TEM observations confirmed the presence of an iH morphology having PI cylinders (light) hexagonally arranged within a PEO–TiO_2 matrix (dark) (Fig. 1k and l). Quantitative TEM measurements indicated a cylinder-to-cylinder spacing of 30 ± 2 nm, compared to the SAXS indicating 36.4 nm. The cylinder diameter and titania wall thickness as determined from TEM measurements were 16 ± 2 nm and 14 ± 1 nm, respectively. Such a large hexagonal structure with thick walls is expected to be thermally more stable than the smaller dimensions typically obtained from Pluronic or KLE polymers (Table 1).

The intermediate samples exhibited mixed morphologies between the two boundary cases of IO28K-h4 and IO28K-h1. The SAXS pattern of sample IO28K-h3 was similar to that of IO28K-h4, but with the addition of a shoulder consistent with the q^* peak of IO28K-h1 (Fig. 1d). TEM images of sample IO28K-h3 contained primarily ~30 nm inverse spherical micelles, similar to sample IO28K-h4, but with added minority domains with iH morphology (Fig. 1e and f). The SAXS pattern of IO28K-h2 was similar to the bimodal pattern of IO28K-h3, but the intensity distribution in the convoluted first peak indicated a decreased content of iSM and an increased content of iH (Fig. 1g). This trend was confirmed by TEM imaging which revealed primarily domains with iH morphology with a minority of ~30 nm iSMs (Fig. 1h and i). The structural analysis of this series of samples indicates a strong morphological dependence on solution conditions during evaporation.

The predominant mechanisms of micelle equilibration, unimer expulsion–insertion and micelle fusion–fission, are dependent upon the interaction strength between the

solvophobic block and the solvent.[88] Although there is still discussion concerning the interplay of these mechanisms,[88–90] the equilibration rates and affecting factors were nonetheless measurable. The exchange kinetics for block copolymer micelles generally range from slow, *i.e.* 1–100 billion times slower than small molecule surfactants,[91] to immeasurably slow.[92–97] The unimer exchange rate was found to depend exponentially on the surface tension penalty for solvophobe–solvent contact.[98,99] Lodge *et al.* recently found that unimer exchange was hypersensitive to the length of the solvophobic chains with a double exponential dependence enabling the precise measurement of polydispersity from the ensemble.[100] For the present study, the differences in morphological behavior could be attributed to the different starting points for solvent compositions before evaporation (Fig. 2b). All samples are expected to increase in water composition during evaporation with the particular starting water composition establishing a trajectory to the final water composition. Therefore, the evolution dynamics and morphology should depend on the selectivity of the solvent mixture during coassembly. The enthalpy associated with solvophobic contacts may be crudely estimated using:

$$X_{12} = \frac{v}{k_b T}(\delta_1 - \delta_2)^2 \quad (1)$$

Here the Flory–Huggins X_{12} parameter for enthalpic 1–2 type contacts scales with the square of the difference of the respective Hildebrand solubility parameters (δ) for components 1 (polyisoprene) and 2 (solvent mixture), as well as the average molecular volume (v), Boltzmann's constant (k_b), and temperature (T). For PI-*b*-PEO in THF–water mixtures, the solutions with higher water content will have higher solubility parameters and thus produce more enthalpic contacts with the solvophobic poly(isoprene) block, inhibiting structural transitions. This rational is consistent with the behavior observed in Fig. 1 where water-rich mixtures prevented the transition from micellar solutions to solid-state equilibrium morphologies. Our rational design strategy for equilibrated morphologies thus requires a low degree of solvophobic interactions at the transition to the solid-state. The solubility parameter for each of the starting mixtures is presented in Fig. 2b. It is straight forward to use eqn (1) to estimate the Flory–Huggins parameter for poly(isoprene) with each of the starting solvent mixtures. However, the crucial composition at the transition from solution to the solid-state is difficult to predict *a priori* due to synergistic evaporative effects such as the formation of positive or negative azeotropes with multi-component systems. The difficulty in predicting solvent composition during evaporation thus makes our design guidelines semi-quantitative.

To further elucidate the structural changes during casting, *in situ* SAXS measurements were performed. Sample IO28K-h1 did not exhibit any scattering patterns in solution until a broad hump appeared 80 minutes after casting (10% retained mass) just prior to becoming a semisolid and then proceeded directly to the iH scattering pattern at the next measurement at 86 minutes (Fig. S1†). Although the temporal resolution was insufficient to elucidate the molecular dynamics, the measurements did indicate that the key period for structure formation is the last minutes of casting as the semisolid films formed.

Considering these findings it is surprising that ordered aluminosilicate morphologies were ever achieved with PI-*b*-PEOs. Typical recipes for such hybrids start with a 5 wt% polymer solution and utilize an inorganic : organic ratio of 2, leading to 12.7 wt% water before hydrolysis and 2.3 wt% water after complete hydrolysis. The apparent insensitivity to water could be due to at least two factors: (1) silicate sols undergo condensation much slower than transition metal oxides which would result in less water release after hydrolysis. (2) Silicate gels formed under acidic conditions tend to exhibit fractal networks with high internal surface areas.[14] Such a porous gel might physisorb much of the free-water from solution, preventing PI-*b*-PEO micellization. Furthermore, these results elucidate the morphological behavior of KLE structure-directing agents, which regardless of inorganic : organic ratio seem to always form spherical micellar morphologies. It is likely that the use of water and alcohol rich solutions to prepare these hybrids leads to trapping the KLE in a selective solvent-induced morphology and preventing the evolution of other morphologies.

Mesoporous materials

The conversion of sample IO28K-h1 to mesoporous crystalline titania was tested employing the CASH procedure described previously in detail.[66] The first calcination of IO28K-h1 was carried out at 700 °C under N_2, leading to sample IO28K-h1-C. The resulting material was black, consistent with the expected carbon residue. SEM images of IO28K-h1-C indicated that the highly ordered iH morphology of IO28K-h1 survived the high temperature treatment (Fig. S2a†). Quantitative measurements from the SEM images indicated an average cylinder-to-cylinder distance of 26.8 ± 3.7 nm with a cylinder diameter of 12.4 ± 2.7 nm and a wall thickness of 12.8 ± 2.0 nm. SAXS measurements similarly confirmed 25.7% shrinkage with a similar cylinder-to-cylinder distance of 27.0 nm (Fig. S2c†). Many coassembled oxide structures have mesostructural compression along the film normal.[28,69,71,72,101,102] This compression complicates SAXS analysis since the orientation of the powdered sample was unknown and thus the longest real-space d_{10} dimension from the elliptical scattering pattern was assumed to coincide with the film normal and was thus used for comparison. Wide angle XRD analysis of IO28K-h1-C confirmed the presence of anatase titania (PDF#21-1272) with a Scherrer average domain size of 9.7 nm calculated from the non-convoluted (101) and (200) peaks (Fig. S2e†). Although the diffraction pattern was dominantly anatase, there was a trace quantity of rutile (PDF#1088-1172). Previous CASH studies on related materials demonstrated a larger extent of rutile with heat treatments as high as 1000 °C.[66] Nitrogen physisorption of IO28K-h1-C exhibited a classic type IV isotherm with an H2 hysteresis loop[18] (Fig. S2h†) indicative of mesopores with restricted pathways (ink bottle). A heterogeneous carbon distribution throughout the cylindrical pores could be the cause of this hysteresis loop. The application of the

BET model led to a calculated overall surface area of 124.7 $m^2\ g^{-1}$. BJH analysis of the adsorption branch led to an average mesopore size of 12.5 nm (Fig. S2i†). The carbon was removed from IO28K-h1-C by heating to 450 °C in air resulting in IO28K-h1-CASH. The white product was consistent with oxidative removal of the carbon. SEM imaging of IO28K-h1-CASH indicated that the ordered iH mesostructure survived removal of the carbon (Fig. S2b†). The analysis of the SEM images indicated a cylinder diameter of 12.7 ± 1.8 nm, a wall thickness of 10.2 ± 1.7 nm, and a cylinder-to-cylinder distance 25.5 ± 3.0 nm. This compares to a cylinder-to-cylinder distance of 25.7 nm as determined by SAXS measurements. The SAXS pattern again contained a broad first-order peak suggesting the preservation of the mesostructure, although higher ordered peaks were no longer detected (Fig. S2d†). Again, wide angle XRD confirmed the presence of anatase titania with a Scherrer average domain size of 10.8 nm and again a trace of rutile. Physisorption analysis of IO28K-h1-CASH exhibited a classical type IV isotherm with a very small hysteresis, consistent with long cylindrical pores of homogeneous diameter (Fig. S2h†). The absence of an H2 hysteresis loop for sample IO28K-h1-CASH indicates that the carbon residue of IO28K-h1-C was partially blocking the mesopores. The application of the BJH model to the adsorption isotherm led to an average mesopore size of 16.1 nm consistent with an additional densification of the titania after carbon removal (Fig. S2i†). The BET analysis was also consistent with this densification indicating a reduced overall surface area of 82.4 $m^2\ g^{-1}$. This data set indicates that the CASH method was successfully applied to the materials described herein.

The previous examples demonstrate that these solubility design principles can guide the formation of ordered mesoporous transition metal oxide structures from highly amphiphilic block copolymers. Exploiting different molar mass PI-*b*-PEOs together with the solubility design guidelines and the CASH method described above enabled unprecedented pore size control in mesoporous crystalline titania. To this end, inverse hexagonal TiO_2–IO hybrid materials were prepared with the same inorganic–organic ratio using different molar mass PI-*b*-PEOs, ranging from 92 to 7 kg mol^{-1}. Indeed, bright field TEM images and SAXS measurements of all hybrids were consistent with highly ordered iH morphologies (Fig. 3). The SAXS spectra show higher order peaks at $(q/q^*)^2 = 4$ and 7 for all hybrid materials while the cylinder-to-cylinder distances decreased from 72.7 to 15.9 nm, consistent with the decrease of the PI-*b*-PEO molar mass.

Highly ordered mesoporous and crystalline titania was synthesized from these hybrids *via* the CASH method. The hybrids were heated to 700 °C and dwelled for 4 h in nitrogen with subsequent calcination at 450 °C in air to yield crystalline titania as confirmed by wide angle XRD analysis. XRD spectra

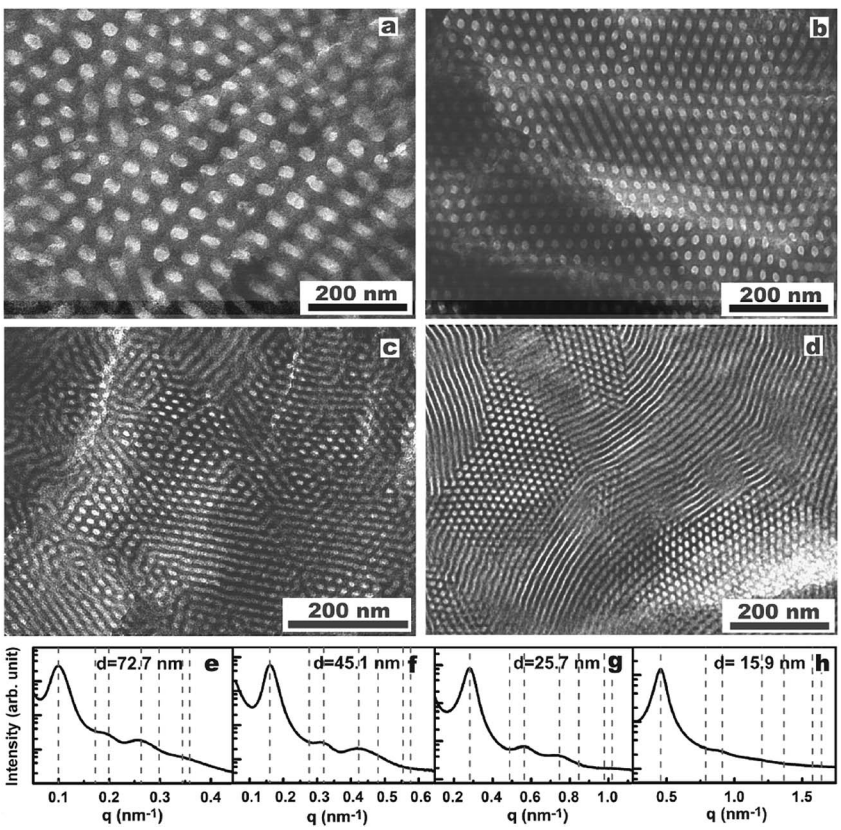

Fig. 3 Bright field TEM images and SAXS patterns for BCP/titania hybrid samples: IO92K-h (a and e), IO41K-h (b and f), IO13K-h (c and g) and IO7K-h (d and h). The SAXS patterns are indexed with a hexagonal lattice. The cylinder-to-cylinder spacing from SAXS measurements were calculated from $d = 4\pi/(q^*\sqrt{3})$ where q^* corresponds to each primary peak.

indicate mostly the anatase phase with a trace amount of rutile for IO92K-CASH, IO41K-CASH and IO13K-CASH samples (Fig. S4†). A purely anatase crystalline phase was achieved by adjusting the temperature and time of the first heat treatment step of the CASH method, as confirmed by the XRD spectra for IO92K-CASH (Fig. 4c), IO41K-CASH, IO13K-CASH and IO7K-CASH (Fig. S5†). Details of the respective heat processing conditions are described in Table S1† showing that block copolymer directed titania can be transformed into highly crystalline and phase-pure anatase upon heat treatments at 600–700 °C for 2–4 h.

The characterization of the largest pore size titania with a highly ordered and crystalline structure is presented in Fig. 4. The SEM images verified the presence of a highly ordered hexagonally arranged cylindrical morphology of the anatase titania after removal of the block copolymer template (Fig. 4a), consistent with TEM results (Fig. S3†). TEM analysis was performed after the brittle titania samples were ground and put on carbon-coated grids. The crushed particles were neither uniform in thickness nor ultrathin and only the edges could be imaged. The highly ordered mesostructure was further confirmed by SAXS analysis showing higher order peaks at $(q/q^*)^2 = 1$, 4 and 7 as in the IO92K-h hybrid material (Fig. 4b). The SAXS cylinder-to-cylinder spacing was determined to be 56.0 nm, indicating a 23% shrinkage upon removal of the block copolymer template from the hybrid material and crystallization of titania (compared to original 72.7 nm) *via* the CASH method. Nitrogen physisorption measurements revealed a narrow pore size distribution with an average pore size of 32.3 nm along with a classical type IV isotherm that is typical of mesoporous materials with a cylindrical pore geometry and a highly uniform pore size distribution (Fig. 4e). The anatase crystallite domain size was calculated to be 11.9 nm using the Scherrer equation.

The structural characteristics of block copolymer derived titania hybrids and the resulting mesoporous crystalline titania with pore size control are summarized in Table 3. The surface areas obtained from BET analysis of nitrogen adsorption–desorption data are high, *i.e.* 64–85 $m^2\ g^{-1}$ for all mesoporous titania. The narrow pore size distributions and the type IV isotherms of titania for IO41K-CASH, IO13K-CASH and IO7K-CASH are consistent with the results described for IO92K-CASH (Fig. S6†). Fig. 5 displays the dependence of SAXS derived *d*-spacings and BJH derived pore sizes on the PI-*b*-PEO molar mass for the various titania/PI-*b*-PEO hybrids and the resulting mesoporous crystalline titania materials ($R^2 > 0.99$) investigated. To the best of our knowledge,[103] we report here the largest pore size to date (32.3 nm) for highly ordered crystalline titania from a block copolymer-inorganic coassembly approach without the use of pore expanding agents.

The solubility design criteria are also generalizable to more complex ABC triblock terpolymers. Poly(isoprene-*b*-styrene-*b*-ethylene oxide) (ISO) was selected since it contains two common hydrophobic blocks, *i.e.*, polyisoprene and polystyrene, and has recently been used for the production of 3D networked aluminosilicate and niobia morphologies with a wide composition window.[72,75] Such networked morphologies have unique advantages in that they have three-dimensional continuity of all three phases and can maintain percolation pathways with lower than 30 vol.% of oxide. Casting solutions were prepared with

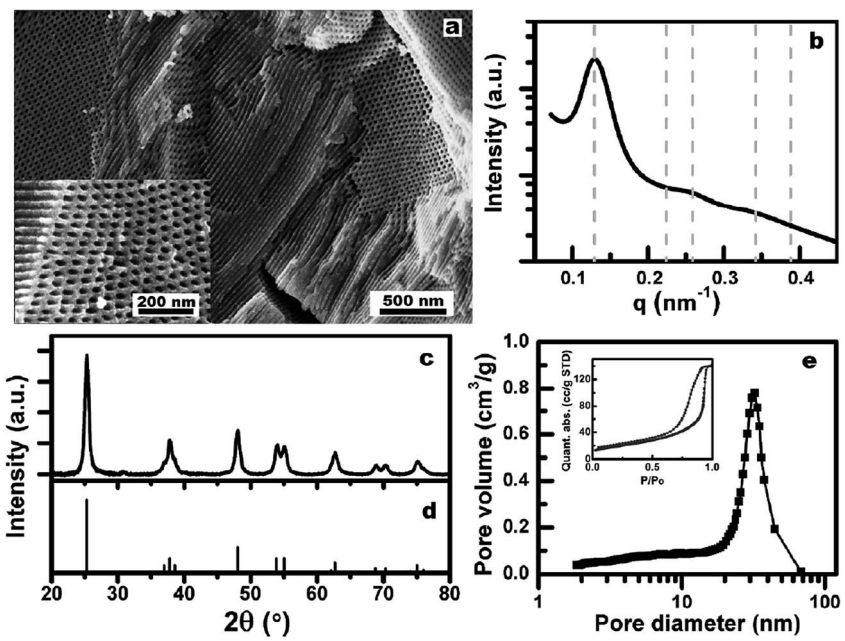

Fig. 4 The ordered mesostructure of IO92K-CASH after the first calcinations in inert atmosphere followed by the subsequent calcination in air is confirmed by SEM (a) and SAXS (b). The cylinder-to-cylinder spacing from SAXS was calculated as 56.0 nm. XRD analysis indicates that the mesoporous titania is highly crystalline (c), with peak assignments consistent with anatase titania (d, PDF#21-1272). Nitrogen physisorption measurements and analysis confirm that this sample is mesoporous with a narrow BJH pore size distribution and average pore size of 32.3 nm (e).

Table 3 Summary of structure characteristics of PI-*b*-PEO derived hybrids and mesoporous titania

BCP/titania hybrids	IO7K-h	IO13K-h	IO28K-h[a]	IO41K-h	IO92K-h
SAXS cylinder-to-cylinder spacing, nm	15.9	25.7	36.4	45.1	72.7
Mesoporous titania	IO7K-CASH	IO13K-CASH	IO28K-CASH	IO41K-CASH	IO92K-CASH
Pore size[b], nm	8.9	11.4	16.1	19.2	32.3
Surface area[c], $m^2\ g^{-1}$	70.0	84.9	82.4	69.2	64.1

[a] Inorganic/organic ratio (2.0) is slightly smaller than the other materials (2.15). [b] Pore size is determined from the peak value of the BJH adsorption derived pore size distribution. [c] surface area is obtained from BET analysis of nitrogen adsorption–desorption data.

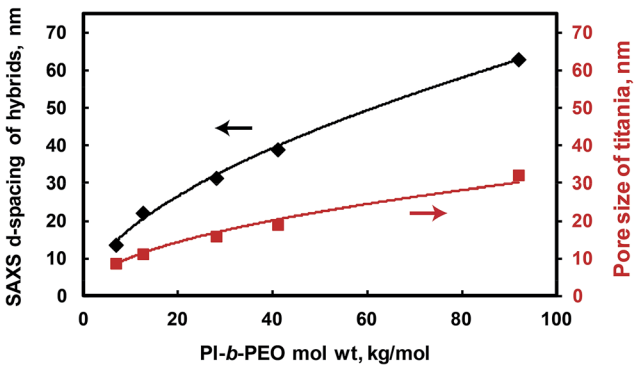

Fig. 5 Dependence of *d*-spacings obtained from SAXS and BJH derived pore sizes on PI-*b*-PEO molar mass for titania/PI-*b*-PEO hybrids and resulting mesoporous crystalline titania, respectively. The *d*-spacing was calculated as $d = 2\pi/q^*$.

very low ~1 wt% water content to enhance the solubility of the hydrophobic blocks during casting (Fig. 2c). The successful production of ordered network morphologies from ISO1 combined with titania sols is demonstrated by sample ISO1–TiO_2. Microtomed sections of this sample clearly show an ordered network connectivity (Fig. 6a and b) with both four-fold and three-fold symmetry, consistent with a cubic network morphology. The SAXS pattern for ISO1–TiO_2 contained two broad peaks that were rather equivocal to interpret directly (Fig. 6c). However, previous experiments with the same ISO1 polymer and niobia sols exhibited a similar scattering pattern and was determined by electron tomography to be consistent with an O^{70} morphology with an equilateral unit cell. Quantitative TEM measurements from these projections yielded a d_{100} spacing of 37–48 nm compared to $d_{100} = 57.0$ nm determined by interpreting the first SAXS peak as d_{110}. Such smaller than expected TEM measurement values have been observed before for similar samples containing low T_g blocks that can reflow after microtoming causing structural distortions.[22,72,75] This discrepancy is notably absent for the comparison of SAXS and electron microscopy data for calcined samples that do not contain polyisoprene, *vide infra*. The titania nanostructures from the coassembly with ISO1 demonstrate that the solubility design guidelines enable the use of complex triblock terpolymers to synthesize highly ordered nanocomposites with novel morphologies.

The crystallization of the ISO1–TiO_2 network was studied with a combination of electron microscopy, SAXS, and XRD. Initial experiments calcining ISO1–TiO_2 indicated that this mesostructure with a minority of oxide is not able to survive high temperature heat treatments. For example, bulk films exhibited significant collapse after heating to 450 °C. We therefore compare heat treatments at 400 °C in N_2 or air, resulting in the samples ISO1–TiO_2–N_2 and ISO1–TiO_2–air, respectively. The mesostructure of both samples survived the heat treatment as evidenced by both SEM images and SAXS observations (Fig. 7a–d). The d_{100} spacing of sample ISO1–TiO_2–N_2 was determined from SAXS and SEM as 45.0 nm and 42.6 ± 4.4 nm, respectively. Sample ISO1–TiO_2–air also had a smaller d_{100} spacing which was measured by SAXS and SEM as 39.5 nm and 40.7 ± 3.0 nm, respectively. The comparison of the SAXS d_{100} spacings indicates that ISO1–TiO_2–N_2 experienced a contraction of 21%, less than the 31% observed for ISO1–TiO_2–air. This is likely due to the *in situ* formation of a carbonaceous hard template as in the CASH procedure. XRD spectra of both

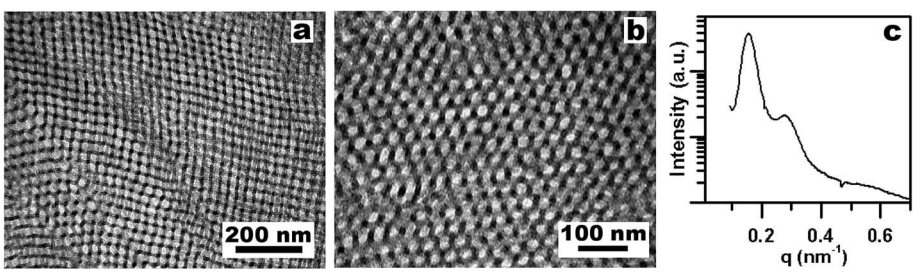

Fig. 6 Bright field TEM images of microtomed sections of ISO1–TiO_2 showing four-fold (a) and three-fold projections (b), consistent with a cubic network morphology. The broad SAXS pattern for ISO1–TiO_2 (c) is similar to a previously reported pattern for networked hybrids derived from the same ISO1 polymer and niobia.

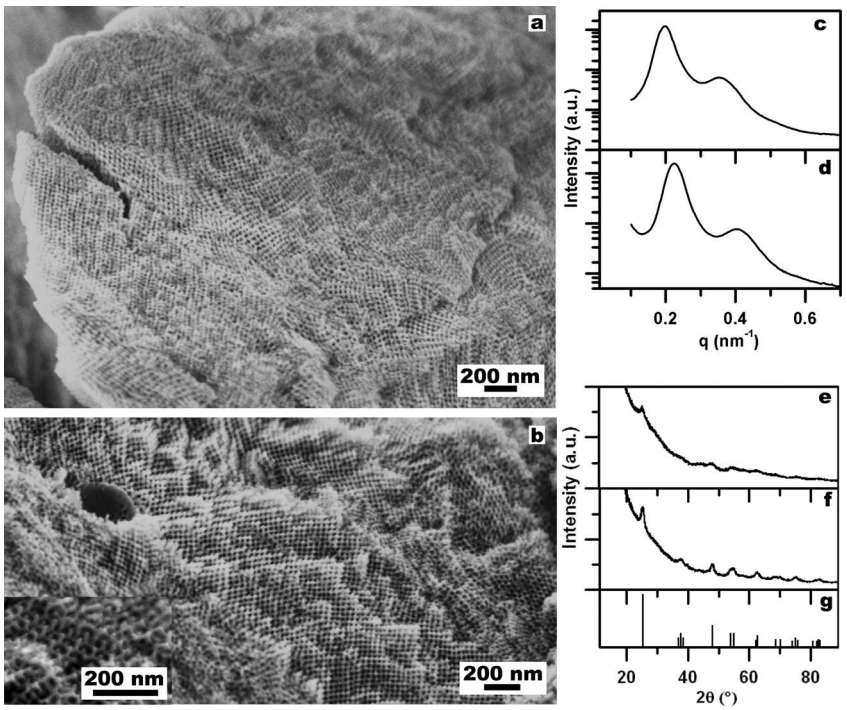

Fig. 7 Sample ISO1–TiO_2 with ordered network mesostructure was calcined at lower temperatures to avoid structural collapse. The mesostructure was preserved after calcination in inert atmosphere as evidenced by SEM (a) and SAXS (c), however, according to XRD (e) the resulting titania is only slightly crystalline. Calcination of ISO1–TiO_2 directly in air results in similar structural preservation as evidenced by SEM (b) and SAXS (d), but results in a greater extent of anatase crystallization as measured by XRD (f and g).

samples were consistent with nanocrystallites of anatase titania (Fig. 5e–g). The low intensity of anatase peaks in sample ISO1–TiO_2–N_2 suggests the presence of a significant amount of amorphous titania. Comparison of the ISO1–TiO_2–N_2 and ISO1–TiO_2–air suggest that the *in situ* formed carbonaceous material constrains the crystallization process by providing a diffusion barrier. Scherrer analysis of the non-convoluted (101) and (200) peaks of ISO1–TiO_2–air indicated an average crystallite size of 7.5 nm. These results suggest that when constrained to lower temperature heat treatments, calcination in air yields more crystalline anatase.[104] We anticipate that such ordered mesoporous networks of crystalline titania will enable better a performance of next generation energy materials.

Conclusions

Solubility design guidelines were established for the development of novel coassembly systems using block copolymer structure-directing agents. This strategy addresses the general challenge of multi-component coassembly with a range of intermolecular interaction strengths. We demonstrated that the evaporation conditions during coassembly play a decisive role in the formation of ordered structures. In the presented examples, the accumulation a water in the solution can trap the assembly in a micellar morphology, preventing the realization of equilibrium block copolymer morphologies. These solubility challenges are exacerbated by the development of more complex and higher molar mass block copolymers. Our semi-quantitative strategy relying on solubility parameters has enabled the manufacture of mesoporous titania with ultra-large pores using a high molar mass IO diblock copolymer as well as a novel titania network morphology by using an ISO triblock terpolymer. In all cases, subsequent calcination treatments enabled the formation of highly crystalline mesoporous materials while preserving the mesostructure.

Acknowledgements

This work was supported by the National Science Foundation Single Investigator Award (DMR-1409105). MS acknowledges the University of South Carolina for startup funds. JS was supported by GS Caltex Corporation in South Korea. SG is grateful for support by the German Academy of Sciences (Leopoldina), Fellowship LPDS2012-13. This work made use of the Cornell Center for Materials Research Shared Facilities, supported through the NSF Materials Research Science and Engineering Centers program (grant DMR 1120296). Some X-ray equipment was supported by Department of Energy grant DE-FG02-11ER16210. CHESS is supported by the NSF and NIH-NIGMS *via* DMR-1332208.

References

1 M. Zukalova, A. Zukal, L. Kavan, M. K. Nazeeruddin, P. Liska and M. Gratzel, Organized mesoporous TiO_2 films exhibiting greatly enhanced performance in dye-sensitized solar cells, *Nano Lett.*, 2005, **5**, 1789–1792.

2 M. Nedelcu, J. Lee, E. J. W. Crossland, S. C. Warren, M. C. Orilall, S. Guldin, S. Huttner, C. Ducati, D. Eder, U. Wiesner, U. Steiner and H. J. Snaith, Block copolymer directed synthesis of mesoporous TiO_2 for dye-sensitized solar cells, *Soft Matter*, 2009, **5**, 134–139.
3 J. M. Szeifert, D. Fattakhova-Rohlfing, D. Georgiadou, V. Kalousek, J. Rathousky, D. Kuang, S. Wenger, S. M. Zakeeruddin, M. Gratzel and T. Bein, "Brick and Mortar" Strategy for the Formation of Highly Crystalline Mesoporous Titania Films from Nanocrystalline Building Blocks, *Chem. Mater.*, 2009, **21**, 1260–1265.
4 P. Docampo, S. Guldin, M. Stefik, P. Tiwana, M. C. Orilall, S. Huttner, H. Sai, U. Wiesner, U. Steiner and H. J. Snaith, Control of Solid-State Dye-Sensitized Solar Cell Performance by Block-Copolymer-Directed TiO_2 Synthesis, *Adv. Funct. Mater.*, 2010, **20**, 1787–1796.
5 S. Guldin, S. Huttner, M. Kolle, M. E. Welland, P. Muller-Buschbaum, R. H. Friend, U. Steiner and N. Tetreault, Dye-Sensitized Solar Cell Based on a Three-Dimensional Photonic Crystal, *Nano Lett.*, 2010, **10**, 2303–2309.
6 L. Li, M. Krissanasaeranee, S. W. Pattinson, M. Stefik, U. Wiesner, U. Steiner and D. Eder, Enhanced photocatalytic properties in well-ordered mesoporous WO(3), *Chem. Commun.*, 2010, **46**, 7620–7622.
7 B. O'Regan and M. Grätzel, A low-cost, high-efficiency solar cell based on dye-sensitized colloidal TiO_2 films, *Nature*, 1991, **353**, 737–740.
8 G. Sudant, E. Baudrin, D. Larcher and J.-M. Tarascon, Electrochemical lithium reactivity with nanotextured anatase-type TiO_2, *J. Mater. Chem.*, 2005, **15**, 1263–1269.
9 Y. Wang, J. Tang, Z. Peng, Y. Wang, D. Jia, B. Kong, A. A. Elzatahry, D. Zhao and G. Zheng, Fully solar-powered photoelectrochemical conversion for simultaneous energy storage and chemical sensing, *Nano Lett.*, 2014, **14**, 3668–3673.
10 W. Li, Z. Wu, J. Wang, A. A. Elzatahry and D. Zhao, A Perspective on Mesoporous TiO Materials, *Chem. Mater.*, 2014, **26**, 287–298.
11 M. C. Orilall and U. Wiesner, Block copolymer based composition and morphology control in nanostructured hybrid materials for energy conversion and storage: solar cells, batteries, and fuel cells, *Chem. Soc. Rev.*, 2011, **40**, 520–535.
12 T. Yanagisawa, T. Shimizu, K. Kuroda and C. Kato, The preparation of alkyltrimethylammonium-kanemite complexes and their conversion to microporous materials, *Bull. Chem. Soc. Jpn.*, 1990, **63**, 988–992.
13 C. T. Kresge, M. E. Leonowicz, W. J. Roth, J. C. Vartuli and J. S. Beck, Ordered Mesoporous Molecular-Sieves Synthesized by a Liquid-Crystal Template Mechanism, *Nature*, 1992, **359**, 710–712.
14 C. J. Brinker and G. W. Scherer, *Sol-gel science: the physics and chemistry of sol-gel processing*, Academic Press, Boston, 1990.
15 Q. S. Huo, D. I. Margolese, U. Ciesla, P. Y. Feng, T. E. Gier, P. Sieger, R. Leon, P. M. Petroff, F. Schuth and G. D. Stucky, Generalized Synthesis of Periodic Surfactant Inorganic Composite-materials, *Nature*, 1994, **368**, 317–321.
16 D. M. Antonelli and J. Y. Ying, Synthesis of Hexagonally Packed Mesoporous TiO_2 by a Modified Sol-Gel Method, *Angew. Chem., Int. Ed. Engl.*, 1995, **34**, 2014–2017.
17 J. Rouquerol, D. Avnir, C. W. Fairbridge, D. H. Everett, J. H. Haynes, N. Pernicone, J. D. F. Ramsay, K. S. W. Sing and K. K. Unger, Recommendations for the Characterization of Porous Solids, *Pure Appl. Chem.*, 1994, **66**, 1739–1758.
18 K. S. W. Sing, D. H. Everett, R. A. W. Haul, L. Moscou, R. A. Pierotti, J. Rouquerol and T. Siemieniewska, Reporting Physisorption Data for Gas Solid Systems with Special Reference to the Determination of Surface-Area and Porosity, *Pure Appl. Chem.*, 1985, **57**, 603–619.
19 N. K. Raman, M. T. Anderson and C. J. Brinker, Template-based approaches to the preparation of amorphous, nanoporous silicas, *Chem. Mater.*, 1996, **8**, 1682–1701.
20 S. A. Bagshaw, E. Prouzet and T. J. Pinnavaia, Templating of Mesoporous Molecular-Sieves by Nonionic Polyethylene Oxide Surfactants, *Science*, 1995, **269**, 1242–1244.
21 P. T. Tanev and T. J. Pinnavaia, A Neutral Templating Route to Mesoporous Molecular Sieves, *Science*, 1995, **267**, 865–867.
22 M. Templin, A. Franck, A. DuChesne, H. Leist, Y. M. Zhang, R. Ulrich, V. Schadler and U. Wiesner, Organically modified aluminosilicate mesostructures from block copolymer phases, *Science*, 1997, **278**, 1795–1798.
23 D. Y. Zhao, J. L. Feng, Q. S. Huo, N. Melosh, G. H. Fredrickson, B. F. Chmelka and G. D. Stucky, Triblock copolymer syntheses of mesoporous silica with periodic 50 to 300 angstrom pores, *Science*, 1998, **279**, 548–552.
24 P. D. Yang, D. Y. Zhao, D. I. Margolese, B. F. Chmelka and G. D. Stucky, Generalized syntheses of large-pore mesoporous metal oxides with semicrystalline frameworks, *Nature*, 1998, **396**, 152–155.
25 G. Wanka, H. Hoffmann and W. Ulbricht, Phase-Diagrams and Aggregation Behavior of Poly(oxyethylene)-Poly(oxypropylene)-Poly(oxyethylene) Triblock Copolymers in Aqueous-Solutions, *Macromolecules*, 1994, **27**, 4145–4159.
26 P. D. Yang, D. Y. Zhao, D. I. Margolese, B. F. Chmelka and G. D. Stucky, Block copolymer templating syntheses of mesoporous metal oxides with large ordering lengths and semicrystalline framework, *Chem. Mater.*, 1999, **11**, 2813–2826.
27 L. Malfatti, M. G. Bellino, P. Innocenzi and G. Soler-Illia, One-Pot Route to Produce Hierarchically Porous Titania Thin Films by Controlled Self-Assembly, Swelling, and Phase Separation, *Chem. Mater.*, 2009, **21**, 2763–2769.
28 E. L. Crepaldi, G. Soler-Illia, D. Grosso, F. Cagnol, F. Ribot and C. Sanchez, Controlled formation of highly organized mesoporous titania thin films: From mesostructured hybrids to mesoporous nanoanatase TiO_2, *J. Am. Chem. Soc.*, 2003, **125**, 9770–9786.

29 D. Grosso, G. Soler-Illia, E. L. Crepaldi, F. Cagnol, C. Sinturel, A. Bourgeois, A. Brunet-Bruneau, H. Amenitsch, P. A. Albouy and C. Sanchez, Highly porous TiO_2 anatase optical thin films with cubic mesostructure stabilized at 700 degrees C, *Chem. Mater.*, 2003, **15**, 4562–4570.
30 S. Y. Choi, M. Mamak, N. Coombs, N. Chopra and G. A. Ozin, Thermally stable two-dimensional hexagonal mesoporous nanocrystalline anatase, meso-nc-TiO_2: Bulk and crack-free thin film morphologies, *Adv. Funct. Mater.*, 2004, **14**, 335–344.
31 B. Smarsly, D. Grosso, T. Brezesinski, N. Pinna, C. Boissiere, M. Antonietti and C. Sanchez, Highly crystalline cubic mesoporous TiO_2 with 10-nm pore diameter made with a new block copolymer template, *Chem. Mater.*, 2004, **16**, 2948–2952.
32 D. Fattakhova-Rohlfing, M. Wark, T. Brezesinski, B. M. Smarsly and J. Rathousky, Highly organized mesoporous TiO_2 films with controlled crystallinity: A Li-insertion study, *Adv. Funct. Mater.*, 2007, **17**, 123–132.
33 T. Brezesinski, J. Wang, J. Polleux, B. Dunn and S. H. Tolbert, Templated Nanocrystal-Based Porous TiO_2 Films for Next-Generation Electrochemical Capacitors, *J. Am. Chem. Soc.*, 2009, **131**, 1802–1809.
34 D. M. Antonelli, Synthesis of phosphorus-free mesoporous titania via templating with amine surfactants, *Microporous Mesoporous Mater.*, 1999, **30**, 315–319.
35 D. Khushalani, O. Dag, G. A. Ozin and A. Kuperman, Glycometallate-surfactants Part 2: non-aqueous synthesis of mesoporous titanium, zirconium and niobium oxides, *J. Mater. Chem.*, 1999, **9**, 1491–1500.
36 G. Soler-Illia and C. Sanchez, Interactions between poly(ethylene oxide)-based surfactants and transition metal alkoxides: their role in the templated construction of mesostructured hybrid organic-inorganic composites, *New J. Chem.*, 2000, **24**, 493–499.
37 D. Grosso, G. Soler-Illia, F. Babonneau, C. Sanchez, P. A. Albouy, A. Brunet-Bruneau and A. R. Balkenende, Highly organized mesoporous titania thin films showing mono-oriented 2D hexagonal channels, *Adv. Mater.*, 2001, **13**, 1085–1108.
38 G. Soler-Illia, E. Scolan, A. Louis, P. A. Albouy and C. Sanchez, Design of meso-structured titanium oxo based hybrid organic-inorganic networks, *New J. Chem.*, 2001, **25**, 156–165.
39 P. C. A. Alberius, K. L. Frindell, R. C. Hayward, E. J. Kramer, G. D. Stucky and B. F. Chmelka, General predictive syntheses of cubic, hexagonal, and lamellar silica and titania mesostructured thin films, *Chem. Mater.*, 2002, **14**, 3284–3294.
40 G. Soler-Illia, A. Louis and C. Sanchez, Synthesis and characterization of mesostructured titania-based materials through evaporation-induced self-assembly, *Chem. Mater.*, 2002, **14**, 750–759.
41 N. Steunou, S. Forster, P. Florian, C. Sanchez and M. Antonietti, Synthesis of nanostructured polymer-titanium oxide composites through the assembly of titanium-oxo clusters and amphiphilic block copolymers micelles, *J. Mater. Chem.*, 2002, **12**, 3426–3430.
42 E. L. Crepaldi, G. Soler-Illia, D. Grosso and M. Sanchez, Nanocrystallised titania and zirconia mesoporous thin films exhibiting enhanced thermal stability, *New J. Chem.*, 2003, **27**, 9–13.
43 O. Dag, I. Soten, O. Celik, S. Polarz, N. Coombs and G. A. Ozin, Solventless acid-free synthesis of mesostructured titania: Nanovessels for metal complexes and metal nanoclusters, *Adv. Funct. Mater.*, 2003, **13**, 30–36.
44 P. C. Angelome, S. Aldabe-Bilmes, M. E. Calvo, E. L. Crepaldi, D. Grosso, C. Sanchez and G. Soler-Illia, Hybrid non-silica mesoporous thin films, *New J. Chem.*, 2005, **29**, 59–63.
45 M. H. Bartl, S. W. Boettcher, K. L. Frindell and G. D. Stucky, 3-D molecular assembly of function in titania-based composite material systems, *Acc. Chem. Res.*, 2005, **38**, 263–271.
46 S. W. Boettcher, M. H. Bartl, J. G. Hu and G. D. Stucky, Structural analysis of hybrid titania-based mesostructured composites, *J. Am. Chem. Soc.*, 2005, **127**, 9721–9730.
47 S. Y. Choi, M. Mamak, S. Speakman, N. Chopra and G. A. Ozin, Evolution of nanocrystallinity in periodic mesoporous anatase thin films, *Small*, 2005, **1**, 226–232.
48 M. Groenewolt, T. Brezesinski, H. Schlaad, M. Antonietti, P. W. Groh and B. Ivan, Polyisobutylene-block-poly(ethylene oxide) for robust templating of highly ordered mesoporous materials, *Adv. Mater.*, 2005, **17**, 1158–2115.
49 H. Shibata, T. Ogura, T. Mukai, T. Ohkubo, H. Sakai and M. Abe, Direct synthesis of mesoporous titania particles having a crystalline wall, *J. Am. Chem. Soc.*, 2005, **127**, 16396–16397.
50 J. Fan, S. W. Boettcher and G. D. Stucky, Nanoparticle assembly of ordered multicomponent mesostructured metal oxides via a versatile sol-gel process, *Chem. Mater.*, 2006, **18**, 6391–6396.
51 M. C. Fuertes and G. Soler-Illia, Processing of macroporous titania thin films: From multiscale functional porosity to nanocrystalline macroporous TiO_2, *Chem. Mater.*, 2006, **18**, 2109–2117.
52 Y. Sakatani, D. Grosso, L. Nicole, C. Boissiere, G. Soler-Illia and C. Sanchez, Optimised photocatalytic activity of grid-like mesoporous TiO_2 films: effect of crystallinity, pore size distribution, and pore accessibility, *J. Mater. Chem.*, 2006, **16**, 77–82.
53 S. W. Boettcher, J. Fan, C. K. Tsung, Q. H. Shi and G. D. Stucky, Harnessing the sol-gel process for the assembly of non-silicate mesostructured oxide materials, *Acc. Chem. Res.*, 2007, **40**, 784–792.
54 W. Y. Dong, Y. J. Sun, C. W. Lee, W. M. Hua, X. C. Lu, Y. F. Shi, S. C. Zhang, J. M. Chen and D. Y. Zhao, Controllable and repeatable synthesis of thermally stable anatase nanocrystal-silica composites with highly ordered hexagonal mesostructures, *J. Am. Chem. Soc.*, 2007, **129**, 13894–13904.
55 O. H. Park, J. Y. Cheng, H. S. Kim, P. M. Rice, T. Topuria, R. D. Miller and H. C. Kim, Formation and

photopatterning of nanoporous titania thin films, *Appl. Phys. Lett.*, 2007, **90**, 3.
56 J. D. Bass, D. Grosso, C. Boissiere and C. Sanchez, Pyrolysis, crystallization, and sintering of mesostructured titania thin films assessed by in situ thermal ellipsometry, *J. Am. Chem. Soc.*, 2008, **130**, 7882–7897.
57 S. Sokolov, E. Ortel and R. Kraehnert, Mesoporous titania films with adjustable pore size coated on stainless steel substrates, *Mater. Res. Bull.*, 2009, **44**, 2222–2227.
58 K. J. Edler, A. M. Hawley, B. M. D. O'Driscoll and R. Schweins, Association of Titania with Nonionic Block Copolymers in Ethanol: The Early Stages of Templating and Film Formation, *Chem. Mater.*, 2010, **22**, 4579–4590.
59 Y. Deng, J. Wei, Z. Sun and D. Zhao, Large-pore ordered mesoporous materials templated from non-Pluronic amphiphilic block copolymers, *Chem. Soc. Rev.*, 2013, **42**, 4054–4070.
60 Y. J. Cheng and J. S. Gutmann, Morphology phase diagram of ultrathin anatase TiO_2 films templated by a single PS-b-PEO block copolymer, *J. Am. Chem. Soc.*, 2006, **128**, 4658–4674.
61 J. Perlich, L. Schulz, M. M. Abu Kashem, Y. J. Cheng, M. Memesa, J. S. Gutmann, S. V. Roth and P. Muller-Buschbaum, Modification of the morphology of P(S-b-EO) templated thin TiO_2 films by swelling with PS homopolymer, *Langmuir*, 2007, **23**, 10299–10306.
62 Y.-J. Cheng, L. Zhi, W. Steffen and J. S. Gutmann, Surface-Supported, Highly Ordered Macroporous Crystalline TiO_2 Thin Films Robust up to 1000 °C, *Chem. Mater.*, 2008, **20**, 6580–6582.
63 J. Zhang, Y. Deng, D. Gu, S. Wang, L. She, R. Che, Z.-S. Wang, B. Tu, S. Xie and D. Zhao, Ligand-Assisted Assembly Approach to Synthesize Large-Pore Ordered Mesoporous Titania with Thermally Stable and Crystalline Framework, *Adv. Energy Mater.*, 2011, **1**, 241–248.
64 Y. Li, W. Luo, N. Qin, J. Dong, J. Wei, W. Li, S. Feng, J. Chen, J. Xu, A. A. Elzatahry, M. H. Es-Saheb, Y. Deng and D. Zhao, Highly ordered mesoporous tungsten oxides with a large pore size and crystalline framework for H_2S sensing, *Angew. Chem., Int. Ed.*, 2014, **53**, 9035–9040.
65 W. Luo, Y. Li, J. Dong, J. Wei, J. Xu, Y. Deng and D. Zhao, A resol-assisted co-assembly approach to crystalline mesoporous niobia spheres for electrochemical biosensing, *Angew. Chem., Int. Ed.*, 2013, **52**, 10505–10510.
66 J. Lee, M. C. Orilall, S. C. Warren, M. Kamperman, F. J. Disalvo and U. Wiesner, Direct access to thermally stable and highly crystalline mesoporous transition-metal oxides with uniform pores, *Nat. Mater.*, 2008, **7**, 222–228.
67 B. C. Garcia, M. Kamperman, R. Ulrich, A. Jain, S. M. Gruner and U. Wiesner, Morphology Diagram of a Diblock Copolymer-Aluminosilicate Nanoparticle System, *Chem. Mater.*, 2009, **21**, 5397–5405.
68 A. C. Finnefrock, R. Ulrich, A. Du Chesne, C. C. Honeker, K. Schumacher, K. K. Unger, S. M. Gruner and U. Wiesner, Metal oxide containing mesoporous silica with bicontinuous "Plumber's Nightmare" morphology from a block copolymer-hybrid mesophase, *Angew. Chem., Int. Ed.*, 2001, **40**, 1207–2120.
69 A. C. Finnefrock, R. Ulrich, G. E. S. Toombes, S. M. Gruner and U. Wiesner, The plumber's nightmare: A new morphology in block copolymer-ceramic nanocomposites and mesoporous aluminosilicates, *J. Am. Chem. Soc.*, 2003, **125**, 13084–13093.
70 A. Jain, G. E. S. Toombes, L. M. Hall, S. Mahajan, C. B. W. Garcia, W. Probst, S. M. Gruner and U. Wiesner, Direct access to bicontinuous skeletal inorganic plumber's nightmare networks from block copolymers, *Angew. Chem., Int. Ed.*, 2005, **44**, 1226–1229.
71 G. E. S. Toombes, A. C. Finnefrock, M. W. Tate, R. Ulrich, U. Wiesner and S. M. Gruner, A re-evaluation of the morphology of a bicontinuous block copolymer-ceramic material, *Macromolecules*, 2007, **40**, 8974–8982.
72 M. Stefik, S. Mahajan, H. Sai, T. H. Epps, F. S. Bates, S. M. Gruner, F. J. DiSalvo and U. Wiesner, Ordered Three- and Five-ply Nanocomposites from ABC Block Terpolymer Microphase Separation with Niobia and Aluminosilicate Sols, *Chem. Mater.*, 2009, **21**, 5466–5473.
73 J. Allgaier, A. Poppe, L. Willner and D. Richter, Synthesis and characterization of poly[1,4-isoprene-b-(ethylene oxide)] and poly[ethylene-co-propylene-b-(ethylene oxide)] block copolymers, *Macromolecules*, 1997, **30**, 1582–1586.
74 S. C. Warren, F. J. Disalvo and U. Wiesner, Nanoparticle-tuned assembly and disassembly of mesostructured silica hybrids, *Nat. Mater.*, 2007, **6**, 156–161.
75 M. Stefik, S. Wang, R. Hovden, H. Sai, M. W. Tate, D. A. Muller, U. Steiner, S. M. Gruner and U. Wiesner, Networked and chiral nanocomposites from ABC triblock terpolymer coassembly with transition metal oxide nanoparticles, *J. Mater. Chem.*, 2012, **22**, 1078–1087.
76 S. J. Gregg and K. S. W. Sing, *Adsorption, Surface Area, & Porosity, Second Edition*, Academic Press, 1982.
77 E. P. Barrett, L. G. Joyner and P. P. Halenda, The Determination of Pore Volume and Area Distributions in Porous Substances. I. Computations from Nitrogen Isotherms, *J. Am. Chem. Soc.*, 1951, **73**, 373–380.
78 J. Brandrup, E. H. Immergut and E. A. Grulke, *Polymer handbook*, Knovel, 1999.
79 L. Chen, B. Yao, Y. Cao and K. Fan, Synthesis of well-ordered mesoporous titania with tunable phase content and high photoactivity, *J. Phys. Chem. C*, 2007, **111**, 11849–11853.
80 M. Arellano, I. Manas-Zloczower and D. L. Feke, Effect of surfactant treatment on the formation of bound polymer on titanium dioxide powders, *Powder Technol.*, 1995, **84**, 117–126.
81 S. Guldin, M. Stefik, H. Sai, U. Wiesner and U. Steiner, *RSC Adv.*, 2015, **5**, 22499–22502.
82 L. E. Manxzer, J. Deaton and P. Sharp, *SchrockR. R. 31. Tetrahydrofuran Complexes of Selected Early Transition Metals*, John Wiley & Sons, Inc., 2007, pp. 135–140.
83 A. Choucair and A. Eisenberg, Control of amphiphilic block copolymer morphologies using solution conditions, *Eur. Phys. J. E: Soft Matter Biol. Phys.*, 2003, **10**, 37–44.

84 R. Lund, L. Willner, J. Stellbrink, A. Radulescu and D. Richter, Role of Interfacial Tension for the Structure of PEP–PEO Polymeric Micelles. A Combined SANS and Pendant Drop Tensiometry Investigation, *Macromolecules*, 2004, **37**, 9984–9993.
85 L. F. Zhang and A. Eisenberg, Multiple morphologies of crew-cut aggregates of polystyrene-b-poly(acrylic acid) block-copolymers, *Science*, 1995, **268**, 1728–1731.
86 L. F. Zhang and A. Eisenberg, Multiple morphologies and characteristics of "crew-cut" micelle-like aggregates of polystyrene-b-poly(acrylic acid) diblock copolymers in aqueous solutions, *J. Am. Chem. Soc.*, 1996, **118**, 3168–3181.
87 Y. S. Yu, L. F. Zhang and A. Eisenberg, Multiple morphologies of crew cut aggregates of polybutadiene-b-poly(acrylic acid) diblocks with low T-g cores, *Langmuir*, 1997, **13**, 2578–2581.
88 T. Haliloglu, I. Bahar, B. Erman and W. L. Mattice, Mechanisms of the exchange of diblock copolymers between micelles at dynamic equilibrium, *Macromolecules*, 1996, **29**, 4764–4771.
89 A. Halperin and S. Alexander, Polymeric Micelles - Their Relaxation Kinetics, *Macromolecules*, 1989, **22**, 2403–2412.
90 E. E. Dormidontova, Micellization kinetics in block copolymer solutions: Scaling model, *Macromolecules*, 1999, **32**, 7630–7644.
91 S. Creutz, J. vanStam, S. Antoun, F. C. DeSchryver and R. Jerome, Exchange of polymer molecules between block copolymer micelles studied by emission spectroscopy. A method for the quantification of unimer exchange rates, *Macromolecules*, 1997, **30**, 4078–4083.
92 K. Schillen, A. Yekta, S. R. Ni and M. A. Winnik, Characterization by fluorescence energy transfer of the core of polyisoprene-poly(methylmethacrylate) diblock copolymer micelles. Strong segregation in acetonitrile, *Macromolecules*, 1998, **31**, 210–212.
93 Y. Y. Won, H. T. Davis and F. S. Bates, Molecular exchange in PEO-PB micelles in water, *Macromolecules*, 2003, **36**, 953–955.
94 S. Jain and F. S. Bates, Consequences of nonergodicity in aqueous binary PEO-PB micellar dispersions, *Macromolecules*, 2004, **37**, 1511–1523.
95 A. G. Denkova, E. Mendes and M. O. Coppens, Non-equilibrium dynamics of block copolymer micelles in solution: recent insights and open questions, *Soft Matter*, 2010, **6**, 2351–2357.
96 R. C. Hayward and D. J. Pochan, Tailored Assemblies of Block Copolymers in Solution: It Is All about the Process, *Macromolecules*, 2010, **43**, 3577–3584.
97 T. Nicolai, O. Colombani and C. Chassenieux, Dynamic polymeric micelles versus frozen nanoparticles formed by block copolymers, *Soft Matter*, 2010, **6**, 3111–3118.
98 L. Willner, A. Poppe, J. Allgaier, M. Monkenbusch and D. Richter, Time-resolved SANS for the determination of unimer exchange kinetics in block copolymer micelles, *Europhys. Lett.*, 2001, **55**, 667–673.
99 R. Lund, L. Willner, D. Richter and E. E. Dormidontova, Equilibrium chain exchange kinetics of diblock copolymer micelles: Tuning and logarithmic relaxation, *Macromolecules*, 2006, **39**, 4566–4575.
100 S. H. Choi, T. P. Lodge and F. S. Bates, Mechanism of Molecular Exchange in Diblock Copolymer Micelles: Hypersensitivity to Core Chain Length, *Phys. Rev. Lett.*, 2010, **104**, 4.
101 M. Klotz, P. A. Albouy, A. Ayral, C. Menager, D. Grosso, A. Van der Lee, V. Cabuil, F. Babonneau and C. Guizard, The true structure of hexagonal mesophase-templated silica films as revealed by X-ray scattering: Effects of thermal treatments and of nanoparticle seeding, *Chem. Mater.*, 2000, **12**, 1721–1728.
102 J. Schuster, R. Kohn, A. Keilbach, M. Doblinger, H. Amenitsch and T. Bein, Two-Dimensional-Hexagonal Periodic Mesoporous Polymer Resin Thin Films by Soft Templating, *Chem. Mater.*, 2009, **21**, 5754–5762.
103 D. Feng, W. Luo, J. Zhang, M. Xu, R. Zhang, H. Wu, Y. Lv, A. M. Asiri, S. B. Khan, M. M. Rahman, G. Zheng and D. Zhao, Multi-layered mesoporous TiO_2 thin films with large pores and highly crystalline frameworks for efficient photoelectrochemical conversion, *J. Mater. Chem. A*, 2013, **1**, 1591.
104 S. Guldin, S. Hüttner, P. Tiwana, M. C. Orilall, B. Ülgüt, M. Stefik, P. Docampo, M. Kolle, G. Divitini, C. Ducati, S. A. T. Redfern, H. J. Snaith, U. Wiesner, D. Eder and U. Steiner, Improved conductivity in dye-sensitised solar cells through block-copolymer confined TiO_2 crystallisation, *Energy Environ. Sci.*, 2010, **4**, 225.
105 I. W. Hamley, V. Castelletto, Z. Yang, C. Price and C. Booth, Melt phase behavior of poly(oxyethylene)-poly(oxypropylene) diblock copolymers, *Macromolecules*, 2001, **34**, 4079–4081.
106 G. Floudas, R. Ulrich and U. Wiesner, Microphase separation in poly(isoprene-b-ethylene oxide) diblock copolymer melts. I. Phase state and kinetics of the order-to-order transitions, *J. Chem. Phys.*, 1999, **110**, 652–663.
107 A. Thomas, H. Schlaad, B. Smarsly and M. Antonietti, Replication of lyotropic block copolymer mesophases into porous silica by nanocasting: Learning about finer details of polymer self-assembly, *Langmuir*, 2003, **19**, 4455–4459.
108 P. F. W. Simon, R. Ulrich, H. W. Spiess and U. Wiesner, Block copolymer-ceramic hybrid materials from organically modified ceramic precursors, *Chem. Mater.*, 2001, **13**, 3464–3486.
109 X. Y. Liu, B. Z. Tian, C. Z. Yu, F. Gao, S. H. Xie, B. Tu, R. C. Che, L. M. Peng and D. Y. Zhao, Room-temperature synthesis in acidic media of large-pore three-dimensional bicontinuous mesoporous silica with Ia3d symmetry, *Angew. Chem. Int. Ed.*, 2002, **41**, 3876–3878.